A generic local thermal equilibrium model for porous reactive materials submitted to high temperatures

CrossMark

J. Lachaud [a,b,*], J.B. Scoggins [c], T.E. Magin [c], M.G. Meyer [d], N.N. Mansour [e]

[a] University of California, Santa Cruz, CA, USA
[b] C la Vie, University of New Caledonia, Noumea, New Caledonia
[c] von Karman Institute, Rhode-Saint-Genése, Belgium
[d] PPME, EA 3325, University of New Caledonia, Noumea, New Caledonia
[e] NASA Ames Research Center, Moffett Field, CA, USA

A B S T R A C T

Many engineering applications involve reacting porous materials submitted to high temperatures. This work presents a detailed but pragmatic heat and mass transfer model for porous materials containing several solid phases and a single gas phase. The detailed chemical interactions occurring between the solid phases and the gas phase are modeled at the pore scale assuming local thermal equilibrium. Homogenized models are obtained for solid pyrolysis, pyrolysis species injection in the gas phase, heterogeneous reactions between the solid phases and the gas phase, and homogeneous reactions in the gas phase. The chemistry models are integrated in a macroscopic model making use of volume-averaged governing equations for the conservation of solid mass, gas mass, species (finite-rate chemistry) or elements (equilibrium chemistry), momentum, and energy. The model has been implemented in the Porous Material Analysis Toolbox based on OpenFoam (PATO), distributed Open Source by NASA. Applications to two high-temperature engineering problems are presented. The first application concerns the design of heat-shields of space vehicles. The second one aims at improving the understanding of biomass pyrolysis for the production of biohydrocarbons.

© 2016 Elsevier Ltd. All rights reserved.

1. Introduction

Modeling of heat and mass transfer phenomena in porous materials is a complex and multifaceted topic. On the one hand, the scientific community has been able to experimentally infer and theoretically derive macroscopic models for simple situations. Darcy's law is a famous example. The direct proportionality between the mass flow rate and the pressure gradient of creeping flows in porous media was experimentally discovered by H. Darcy in the 19th century [1] and mathematically justified a couple of decades ago [2,3]. There is a rich literature of problems that have been understood, modeled using upscaling theories, and experimentally verified. They are now available in textbooks – for example, to cite a few of them: diffusion in porous media [4], convection in porous media [5], radiation in porous media [6]. Each particular field is the object of active research aiming at improving the theory for the derivation of macroscopic models and refining the experimental capabilities to measure parameters [7–10]. Computed

micro-tomography and direct numerical simulations (DNS) can, in some cases, usefully complement traditional upscaling and experimental analyses [8,11,12]. On the other hand, there is a large range of complex multi-physics problems for which detailed mathematical derivations lead to non-practical models and experimental or DNS analyses are difficult. Models are therefore either empirical, heuristic, or based on an upscaling theory with some assumptions, typically neglecting couplings between most phenomena for practical reasons. This is in particular the case for reactive porous materials submitted to high-temperatures. Typical high-temperature engineering applications involving chemical reactions are heat shields of space vehicles using ablative materials [13–15] or transpiration cooling [16], nozzle's walls of rockets [17–19], carbonization of pyrolyzing porous materials like biomass [20–23], cracking of hot gases passing through a porous material [24–26], chemical vapor infiltration and deposition [27,28], ..., to simple burning of a match.

From a material point of view, there are more similarities than differences between the applications cited, even between the porous heat-shield of a space vehicle entering an atmosphere at hypersonic speed and a match burning (Fig. 1). In most cases,

---

Nomenclature

Latin

c_p	specific heat, $J \cdot kg^{-1} \cdot K^{-1}$
A_i	species i
$\mathcal{A}_{i,j}$	Arrhenius law pre-exponential factor, *SI*
e	specific energy, $J \cdot kg^{-1}$
$\mathcal{E}_{i,j}$	Arrhenius law activation energy, $J \cdot mol^{-1}$
$\mathcal{F}$	effective diffusion flux, $kg \cdot m^{-2} \cdot s^{-1}$
$F_{i,j}$	fraction of subphase j in phase i
h	specific absolute enthalpy, $J \cdot kg^{-1}$
$\mathbf{K}$	permeability tensor, m^2
$\overline{\overline{\mathbf{k}}}$	conductivity tensor, $J \cdot m^{-2} \cdot s^{-1} \cdot K^{-1}$
$\overline{k}_r$	reaction rates, *SI*
$\mathcal{M}$	molar mass, $kg \cdot mol^{-1}$
$m_{i,j}$	Arrhenius law parameter
$n_{i,j}$	Arrhenius law parameter
N_g	number of gaseous species
N_p	number of solid phases
p	pressure, Pa
P_i	number of subphases in solid phase i
$\mathcal{Q}$	effective diffusion heat flux, $J \cdot m^{-2} \cdot s^{-1}$
$\mathcal{R}$	perfect gas constant, $J \cdot mol^{-1} \cdot K^{-1}$
s	specific surface, $m^2 \cdot m^{-3}$
$\mathbf{v}$	convection velocity, $m \cdot s^{-1}$
$\mathbf{x}, \mathbf{y}$	space variables, respectively macroscopic and local.
X	molar density, $mol \cdot m^{-3}$
y	species mass fractions
z	element mass fractions

Greek

β	Klinkenberg tensor, Pa
$\overline{\overline{\epsilon}}$	volume fraction
η	tortuosity
ζ	mass stoichiometric coefficient
θ	active site density, $mol \cdot m^{-3}$
μ	viscosity, $Pa \cdot s$
ν	stoichiometric coefficients
Π	pyrolysis gas production rate, $kg \cdot m^{-3} \cdot s^{-1}$
π_k	pyrolysis production rate of species/element k, $kg \cdot m^{-3} \cdot s^{-1}$
ρ	density, $kg \cdot m^{-3}$
$\chi_{i,j}$	advancement of pyrolysis reaction j within phase i
ψ	generic variable
ω	production rate, $mol \cdot m^{-3} \cdot s^{-1}$
Ω_h	overall heterogeneous mass reaction rate, $kg \cdot m^{-3} \cdot s^{-1}$
ω_i^h	effective heterogeneous mass reaction rate of phase i, $kg \cdot m^{-3} \cdot s^{-1}$

Subscripts

|	
g	Gas phase
p	Solid phase
t	Solid and gas phases

external flow conditions only affect the internal behavior of a porous material through boundary conditions at the material/environment interface. The conservation laws within the materials are essentially the same and the same mathematical model may be used to analyze their behaviors. In the literature, we find different types of notations and simplifying hypotheses for the different applications but they rely on the same physics and base model, with of course sometimes additional features required for some applications. The motivation of this article is to provide a detailed physics-based framework for engineering analyses and simulations. It contains all the base features needed to model the high-temperature applications mentioned, with a special effort to detail the chemistry. The following heat and mass transport phenomena are modeled: pyrolysis, pyrolysis species production, homogeneous and heterogeneous reactions (equilibrium or finite-rate), species transport by convection and diffusion, momentum conservation in porous media, and energy conservation. To keep the model generic and pragmatic, we assume local thermal equilibrium and local chemical homogeneity in the gas phase. A

numerical simulation tool implementing this model is released open source.

The article is organized as follows. In section two, we present a generic local thermal equilibrium model for decomposing and reacting porous materials, containing several solid phases and a single gas phase in the continuum regime (small Knudsen number). In section three, the model capabilities are illustrated with the analysis of two diverse applications. The first one concerns the analysis of the thermal response of the ablative heat-shield of a space vehicle. The second one aims at improving the understanding of biomass pyrolysis for the production of green energy. Section four provides a summary and points the reader to an implementation of the formulation available open source.

2. Model

In this section, we present a generic local thermal equilibrium model for decomposing and reacting porous materials, containing several solid phases and a single gas phase. The governing
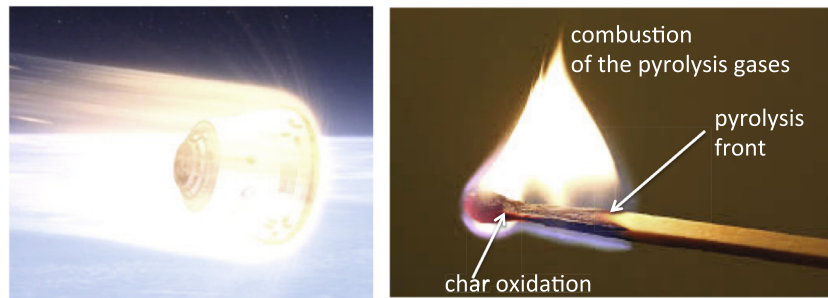
a) atmospheric entry of a space vehicle (high-temperature, high-speed flow)

b) match burning

Fig. 1. Two high-temperature reactive porous medium applications.

equations for the gasification of the solid phases, gas and elements/species conservations, momentum conservation, and energy conservation are presented in the following subsections.

2.1. Hypotheses and notations

As mentioned in the introduction, several upscaling theories have been developed. The most popular in the field of porous media are: the homogenization theory [2], the volume-averaging technique [4], and stochastic methods [29]. Theses different approaches lead to equivalent results as long as the same physical hypotheses and the same level of mathematical approximations are used [7].

In this work, we have chosen to use unmarked notations – not attached to a particular upscaling theory. The choice has been made to use both intrinsic phase variables, noted with a phase index i, and effective variables, noted without index. Using, for example, the volume-averaging approach, intrinsic phase variables are defined as

$$\psi_i = \psi_i(\mathbf{x}, t) = \frac{1}{V_i} \int_{V_i} \psi_i^*(\mathbf{x} + \mathbf{y}, t) \, d\mathbf{y} \tag{1}$$

where ψ_i^* is the local value of a physical variable, i is a phase index, $\mathbf{x}$ is the macroscopic coordinate, $\mathbf{y}$ is the local coordinate within the averaging volume V, and V_i is the volume of phase i within the averaging volume. The models rely on the hypothesis of scale separation, implying the existence of a representative elementary volume (REV), where the small scale variations are smoothed, as illustrated in Fig. 2.

The volume fraction of each phase i is computed using the phase indicator γ_i, with $\gamma_i = 1$ within phase i, and $\gamma_i = 0$ outside of phase i such that

$$\epsilon_i = \epsilon_i(\mathbf{x}, t) = \frac{1}{V} \int_V \gamma_i(\mathbf{x} + \mathbf{y}, t) \, d\mathbf{y} \tag{2}$$

where V is the averaging volume.

The averaged values of extensive variables (volume, mass, energy) are obtained by weighted summation of intrinsic phase values. For example, the total local density ρ of a porous material, filled with gas and containing N_p solid phases, is given by

$$\rho = \epsilon_g \rho_g + \sum_{i \in [1, N_p]} \epsilon_i \rho_i = \sum_{i \in [0, N_p]} \epsilon_i \rho_i \tag{3}$$
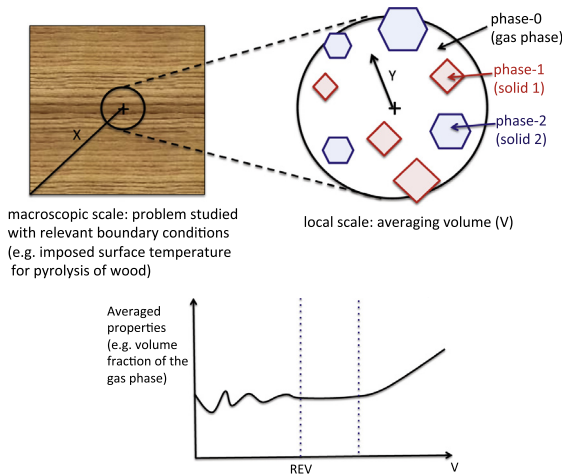

Fig. 2. Illustration of the volume averaging approach: (a) simplified notation for the three-dimensional space coordinates: **x**: macroscopic scale, **y**: local scale. (b) hypothesis of scale separation.

where phase $i = 0$ is taken to be the gas. The summation rule is used to derive the models described in the following subsections. Unfortunately, this rule is generally not applicable for intensive variables (pressure, velocity, temperature) and for parameters that describe phenomena involving intensive variables (tortuosity, permeability, conductivity). For the intensive variables, classical upscaling derivations are used.

2.2. Gasification of the solid phases and species produced

In this subsection, we present a generic model for the local mass transfer occurring between solid and gas phases. The N_p solid phases may lose mass by pyrolysis and exchange mass with the surrounding gas through heterogeneous reactions and phase changes.

2.2.1. Pyrolysis

Each solid phase p_i may decompose following several pyrolysis kinetics. It is a common practice to split each phase i into P_i subphases to model its different degradation mechanisms [13]. For example, the main components of the wood-cell walls (cellulose, hemicellulose, and lignin) are usually modeled as three phases, and the polymer chains of cellulose themselves decompose following several pyrolysis mechanisms [22]. The decomposition of subphase j (from solid phase i) produces the elements/species A_k according to the stoichiometric coefficients $\zeta_{i,j,k}$, as follows

$$p_{i,j} \to \sum_{k \in [1, N_g]} \zeta_{i,j,k} A_k, \quad \forall i \in [1, N_p], \ \forall j \in [1, P_i], \tag{4}$$

where N_g is the total number of gaseous element/species accounted for in the gas mixture. The choice of using elements or species is dictated by the type of chemistry model that is used in the gas phase (elements for equilibrium chemistry and species for finite-rate chemistry).

The advancement $\chi_{i,j}$ (varying from 0 to 1) of the pyrolysis reaction of subphase j within phase i is modeled using Arrhenius laws of the general form

$$\frac{\partial_t \chi_{i,j}}{(1 - \chi_{i,j})^{m_{i,j}}} = T^{n_{i,j}} \mathcal{A}_{i,j} \exp\left(-\frac{\mathcal{E}_{i,j}}{\mathcal{R}T}\right), \quad \forall i \in [1, N_p], \ \forall j \in [1, P_i]. \tag{5}$$

The total production rate of species/element k by decomposition of the solid is obtained by summation of the productions of the N_p phases

$$\pi_k = \sum_{i \in [1, N_p]} \sum_{j \in [1, P_i]} \zeta_{i,j,k} \epsilon_{i,0} \rho_{i,0} F_{i,j} \partial_t \chi_{i,j} \tag{6}$$

where $\epsilon_{i,0}$, $\rho_{i,0}$, and $F_{i,j}$, are respectively the initial (at $t = 0$) volume fraction of phase i, intrinsic density of phase i, and mass fraction of subphase j within phase i.

The overall pyrolysis-gas production rate is obtained by summing over k and reads

$$\Pi = \sum_{k \in [1, N_g]} \pi_k \tag{7}$$

2.2.2. Heterogeneous reactions and phase changes: coupling with homogeneous chemistry in the pores

Chemistry mechanisms are described using a set of N_r chemical reactions that writes

$$\sum_{i=1}^{N_s} v'_{ri} A_i \underset{k''_r}{\overset{k'_r}{\rightleftharpoons}} \sum_{j=1}^{N_s} v''_{rj} A_j \quad \forall r \in [1, N_r] \tag{8}$$

where N_s is the total number of species. Very often, solid and gas species are modeled using different models. We propose a unified approach.

For elementary reactions, species production rates are modeled using

$$\omega_i = \sum_{r=1}^{N_r} \left[(v''_{ri} - v'_{ri}) \left(k'_r \prod_{j=1}^{N_s} (X_j)^{v'_{rj}} - k''_r \prod_{j=1}^{N_s} (X_j)^{v''_{rj}} \right) \right] \quad (9)$$

where X_j is the averaged molar density of species j. Non-elementary reactions may be modeled using molar density exponents that are not equal to the molecularity, or additional terms can be added, for example to account for third body reactions or pressure fall-off.

To model heterogenous chemistry, the effective molar density of a reacting solid phase i may be conveniently modeled as [30]

$$X_i = \frac{s_i \theta_i}{\epsilon_g} \quad (10)$$

where s_i is its specific surface and θ_i its active site density. This allows introducing the solid phases in the homogeneous chemistry mechanism, to solve homogeneous and heterogeneous finite-rate chemistry in a coupled manner, and compute the effective reaction rates with improved accuracy and numerical stability.

High-temperature engineering applications often involve sublimation, which is not a chemical reaction but a change of phase. However, for convenience, sublimation can be integrated in the same formalism after some mathematical transformations as explained in Appendix A.

In the case of equilibrium chemistry, infinite reaction rates may be considered to lead to chemical equilibrium. However, in this case, it is more efficient to use Gibbs minimization technique to compute the equilibrium species composition based on elemental composition, pressure and temperature [31,32,15].

2.2.3. Mass balance equations for the solid phases

The average mass evolution for each solid phase is obtained by summing over pyrolysis and heterogeneous reaction contributions

$$-\partial_t(\epsilon_i \rho_i) = \sum_{j \in [1,P_i]} \epsilon_{i,0} \rho_{i,0} F_{i,j} \partial_t \chi_{i,j} + \omega_i^h \quad (11)$$

where ω_i^h is the heterogeneous production rate of the species of phase i obtained by summing over the relevant contributions in Eq. (9).

Possible structural changes, separately affecting ϵ_i and ρ_i, depend on the type of phenomena and materials involved and need to be assessed on a case-by-case basis. Also, terms accounting for shrinkage or swelling (due to temperature variations, for example) may be added. In this latter case, solid flux divergence terms need to be added in the conservation equations to conserve mass and energy.

The total mass change rate of the solid due to heterogeneous reactions reads

$$\Omega_h = \sum_{i \in [1,N_p]} \omega_i^h \quad (12)$$

2.3. Mass conservation: gas, species/elements

The gaseous mass conservation equation includes production terms (right hand side) to account for the exchange with the surrounding gas and reads

$$\partial_t(\epsilon_g \rho_g) + \partial_{\mathbf{x}} \cdot (\epsilon_g \rho_g \mathbf{v_g}) = -\sum_{i \in [1,N_p]} \partial_t(\epsilon_i \rho_i) = \Pi + \Omega_h \quad (13)$$

The conservation equations for either the N_g^e elements or N_g^s species mass fractions need to be resolved to accurately model element or species transport and chemistry within the pores of the material. Element conservation is used under the equilibrium chemistry assumption. Species conservation is used together with finite-rate (non equilibrium) chemistry models. The conservation equations for the species mass fractions y_i (finite-rate chemistry) read [33]

$$\partial_t(\epsilon_g \rho_g y_i) + \partial_{\mathbf{x}} \cdot (\epsilon_g \rho_g y_i \mathbf{v_g}) + \partial_{\mathbf{x}} \cdot \mathcal{F}_i = \pi_i + \epsilon_g \omega_i \mathcal{M}_i, \quad \forall i \in N_g^s, \quad (14)$$

and the conservation equations for the element mass fractions z_k (equilibrium chemistry) read

$$\partial_t(\epsilon_g \rho_g z_k) + \partial_{\mathbf{x}} \cdot (\epsilon_g \rho_g z_k \mathbf{v_g}) + \partial_{\mathbf{x}} \cdot \mathcal{F}_k = \pi_k, \quad \forall k \in N_g^e. \quad (15)$$

Under the equilibrium chemistry assumption, the species gas composition is directly computed from the local elemental composition, temperature, and pressure using Gibbs minimization technique [31,32,15]. $\mathcal{F}_i$ and $\mathcal{F}_k$ are the effective multicomponent diffusion mass fluxes [4] of the ith species and kth element. The species diffusion fluxes sum to zero and therefore do not appear in the total mass balance in Eq. (13). The effective species diffusion fluxes may be obtained by various state-of-the art methods [8]. Effective element diffusion fluxes are then obtained by linear combination of the species (physical) fluxes. In Appendix B, we present a model that directly provides the element or the species effective multi-component diffusion fluxes.

2.4. Momentum conservation

The average gas velocity is obtained by resolution of the momentum-conservation equation. In porous media, the volume-averaged momentum conservation may be written as [1–3]

$$\mathbf{v_g} = -\frac{1}{\epsilon_g} \left(\frac{1}{\mu} \underline{\underline{\mathbf{K}}} + \frac{1}{p} \underline{\underline{\beta}} \right) \cdot \partial_{\mathbf{x}} p \quad (16)$$

Most of the materials are anisotropic, therefore, the permeability – $\underline{\underline{\mathbf{K}}}$ – is a second order tensor. The contribution $\underline{\underline{\beta}}$ is the Klinkenberg correction to account for slip effects (at the pore scale) when the Knudsen number (ratio of the mean free path to the mean pore diameter) is not very small. When the Reynolds number within the pores becomes large in the continuum regime, high velocity effects are observed, leading to flow separation at the pore scale. We did not include it in our model but this could be done if needed using for example the Forchheimer correction [10].

The Darcian velocity may be introduced in the gas mass conservation to read

$$\partial_t(\epsilon_g \rho_g) - \partial_{\mathbf{x}} \cdot \left(\rho_g \left(\frac{1}{\mu} \underline{\underline{\mathbf{K}}} + \frac{1}{p} \underline{\underline{\beta}} \right) \cdot \partial_{\mathbf{x}} p \right) = \Pi + \Omega_h \quad (17)$$

which, under the assumption that the perfect gas law holds, rewrites

$$\partial_t \left(\frac{\epsilon_g \mathcal{M}}{\mathcal{R}T} p \right) - \partial_{\mathbf{x}} \cdot \left(\frac{p\mathcal{M}}{\mathcal{R}T} \left(\frac{1}{\mu} \underline{\underline{\mathbf{K}}} + \frac{1}{p} \underline{\underline{\beta}} \right) \cdot \partial_{\mathbf{x}} p \right) = \Pi + \Omega_h \quad (18)$$

where $\mathcal{M}$ is the mean molar mass of the gas mixture.

There are clear advantages in solving directly this equation in pressure, which is a commonly available boundary condition, rather than handling separately Eqs. (13) and (16) and the perfect gas law. A discussion on boundary conditions is included in Appendix C.

2.5. Energy conservation

Under the local thermal equilibrium assumption, the energy conservation may be written as [7]

$$\partial_t(\rho_t e_t) + \partial_{\mathbf{x}} \cdot (\epsilon_g \rho_g h_g \mathbf{v_g}) + \partial_{\mathbf{x}} \cdot \sum_{k=1}^{N_g} (\mathcal{Q}_k)$$

$$= \partial_{\mathbf{x}} \cdot (\underline{\underline{\mathbf{k}}} \cdot \partial_{\mathbf{x}} T) + \mu \epsilon_g^2 (\underline{\underline{\mathbf{K}}}^{-1} \cdot \mathbf{v_g}) \cdot \mathbf{v_g} \quad (19)$$

where the total (storage) energy of the porous medium is the sum of the energy of its phases

$$\rho_t e_t = \epsilon_g \rho_g e_g + \sum_{i \in [1,N_p]} \epsilon_i \rho_i h_i \tag{20}$$

The second terms of the left-hand side is the heat convection term, where h_g is the absolute enthalpy of the gas mixture. The third term models heat transport by effective diffusion of the species. Its detailed expression is provided in Appendix B. The second term on the right-hand side is the energy dissipated by viscous effects in the Darcian regime [34]. It is very small and can be neglected. Heat transfer is conveniently modeled as an effective diffusive transfer (Fourier's law). The effective conductivity – $\underline{\mathbf{k}}$ – is a second order tensor accounting for conduction in the solid, conduction in the gas, radiative heat transfer, including possible coupling terms between these heat transfer modes and deviation by coupling with other terms. On a case-by-case basis, more advanced and accurate models can be derived [6,35]. According to Puiroux et al. [14], solid and gas phases are in thermal equilibrium as long as the Peclet number for diffusion of heat within the pores is small ($Pe = \epsilon_g \rho_g c_{p,g} d_p v_g / k_g$). It is important to mention that strong enthalpy changes in the solid phases may also lead to thermal non-equilibrium, this time between the solid phases themselves.

Effective conductivity is generally the main mode of heat transport. To solve implicitly Eq. (19), it is therefore convenient to develop it and express it in terms of temperature. The first term reads

$$\partial_t(\rho_t e_t) = \partial_t(\epsilon_g \rho_g e_g) + \sum_{i \in [1,N_p]} \partial_t(\epsilon_i \rho_i h_i) \tag{21}$$

$$= \partial_t(\epsilon_g \rho_g (h_g - p/\rho_g)) + \sum_{i \in [1,N_p]} [\epsilon_i \rho_i c_{p,i} \partial_t T + h_i \partial_t(\epsilon_i \rho_i)] \tag{22}$$

Eq. (19) can then be rearranged as follows

$$\sum_{i \in [1,N_p]} [(\epsilon_i \rho_i c_{p,i}) \partial_t T] - \partial_\mathbf{x} \cdot (\underline{\mathbf{k}} \cdot \partial_\mathbf{x} T) = \begin{vmatrix} - \sum_{i \in [1,N_p]} h_i \partial_t(\epsilon_i \rho_i) \\ -\partial_t(\epsilon_g \rho_g h_g - \epsilon_g p) + \partial_\mathbf{x} \cdot (\epsilon_g \rho_g h_g \mathbf{v_g}) \\ + \partial_\mathbf{x} \cdot \sum_{k \in [1,N_g]} (Q_k) + \mu \epsilon_g^2 (\underline{\mathbf{K}}^{-1} \cdot \mathbf{v_g}) \cdot \mathbf{v_g} \end{vmatrix} \tag{23}$$

and implicitly solved in temperature, possibly lagging the right-hand side terms.

3. Applications

In this section, two applications are presented: ablative heat-shield design and valorization of biomass by pyrolysis. Despite the obvious differences in material properties and environmental conditions, the same generic model presented above may be used for these applications. The generic model has been implemented in the Porous Material Analysis Toolbox based on OpenFoam (PATO) [36,15]. First-order implicit finite-volume schemes in time and space [37,38], which have been shown to provide excellent convergence and accuracy [36,15], were used for the simulations.

3.1. Ablative heat-shield design

Space exploration missions often include entering a planetary atmosphere at hypersonic speed. A high enthalpy hypersonic shock forms around the spacecraft and kinetic energy is progressively dissipated into heat [39]. Heat is transferred to the surface of the spacecraft by radiation and convection. A suitable heat shield is needed to protect the payload. The level of heat flux increases with entry speed and atmospheric density. For fast hypersonic entries,

typically faster than 8 km/s from earth orbit, ablative materials are used as Thermal Protection Systems (TPS). These materials mitigate the incoming heat through phase changes, chemical reactions, and material removal [40]. Low-density porous carbon/phenolic composites are being used for space exploration missions [41,42]. They are made of a carbon fiber preform partially impregnated with phenolic resin. They are very light with an overall density around 200 kg/m^3, are good insulators, and display sufficient mechanical properties for blunt body atmospheric entry.

During atmospheric entry, carbon/phenolic materials undergo thermal degradation and ultimately recession captured by the following physico-chemical phenomena (Fig. 3). The phenolic polymer thermally decomposes and progressively carbonizes into a low density carbon form, losing mass while releasing pyrolysis gases – hydrogen and phenol are shown as examples in Fig. 3. The pyrolysis gases percolate and diffuse to the surface through the network of pores. Reactions within the pyrolysis-gas mixture (homogeneous reactions) and between pyrolysis gases and the char take place with possible coking effects (heterogeneous reactions). Mixing and reaction of the pyrolysis gases with boundary layer gases into the pores of the material occur when boundary layer gases penetrate in the material by forced convection or due to fast diffusion at low pressures [15]. At the surface, the material is removed by ablation and the outer surface recedes. Depending on entry conditions, ablation may be caused by heterogeneous chemical reactions (oxidation, nitridation), phase change (sublimation), and possibly mechanical erosion (often called spallation).

A review of the open literature has revealed three levels of models used in twenty-five numerical simulation tools [43]. The first modeling level (1) was initially developed for dense ablators in the 1960s [44]. It is currently implemented in lead design codes [45]. The core phenomena of the pyrolysis/ablation problem are modeled but many simplifications are used. A major simplification is that the momentum-conservation is not implemented, meaning that the direction of the pyrolysis gas flow and the internal pressure need to be arbitrarily prescribed by the user. This type (1) model is well adapted for unidimensional, quasi steady-state, and equilibrium chemistry conditions with constant element fractions. Type (1) models [44,46,47] have enabled successful porous heat-shield design but have required the use of large safety margins to compensate for possible prediction errors [42]. The second level (2) of modeling includes the implementation of the momentum conservation. This capability is found in a few design codes and in several recent analysis codes allowing the determination of gas flow directions for constant element/species mixtures. Type (3) models include element or species conservation equations, and associated equilibrium or finite-rate chemistry models, for a more rigorous modeling of heat and mass transport phenomena.The model presented in this article is comparable with advanced finite-rate chemistry [36] and advanced equilibrium chemistry [15] ablation Type (3) models recently developed. Both hypotheses, finite-rate and equilibrium chemistry, have been synthesized in a single more general model in this work.

We propose to compare the behavior of a low-density carbon/phenolic composite when modeled with the type 1 approach using the state-of-the-art code FIAT [45] and the type 3 approach using PATO in finite-rate chemistry mode. The material of the study is the Theoretical Ablative Composite for Open Testing (TACOT). Its composition and properties are comparable to NASA's Phenolic Impregnated Carbon Ablator [48]. In volume, TACOT is made of 10% of carbon fibers (phase-1), 10% of phenolic resin (phase-2), and is 80% porous (phase-0: gas). Therefore, in the generic model presented in the previous section, we use $N_p = 2$. Phenolic resin is known to decompose following several parallel pyrolysis mechanisms [36], as shown in Table 1. Phase 2 contains then 4 subphases.
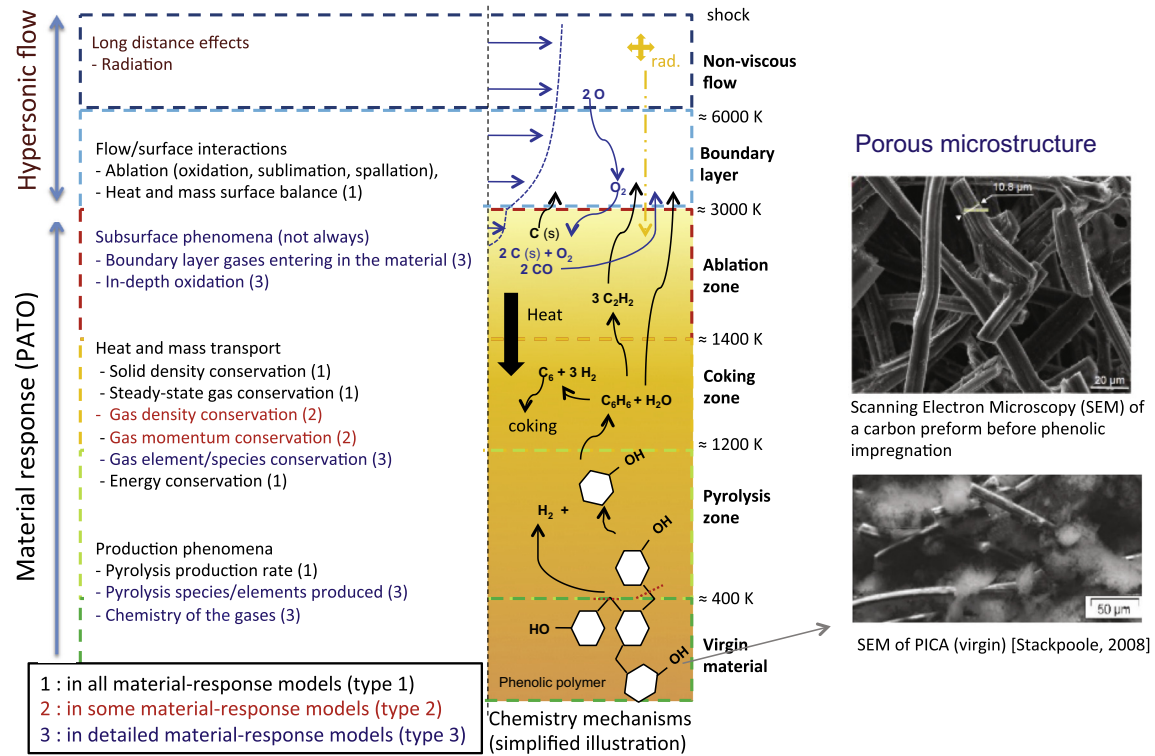
Fig. 3. Phenomenology of porous carbon/phenolic ablative materials.

Table 1
Pyrolysis balance equations and kinetic parameters.

j	Pyrolysis of phenolic matrix	Peak (K)	$F_{2,j}$	$A_{2,j}$	$E_{2,j}$	$m_{2,j}$	$n_{2,j}$
1	$p_{2,1} \rightarrow H_2O(physisorbed)$	373	0.01	$8.56 \cdot 10^3$	$7.12 \cdot 10^4$	3	0
2	$p_{2,2} \rightarrow 0.69H_2O + 0.01C_6H_6$ $+0.01C_7H_8 + 0.23C_6H_6O$	773	0.24	$8.56 \cdot 10^3$	$7.12 \cdot 10^4$	3	0
3	$p_{2,3} \rightarrow 0.09CO_2 + 0.33CO + 0.58CH_4$	873	0.03	$4.98 \cdot 10^8$	$1.70 \cdot 10^5$	3	0
4	$p_{2,4} \rightarrow H_2$	1073	0.06	$4.98 \cdot 10^8$	$1.70 \cdot 10^5$	3	0

For the graphical illustration, we use a case presented with more details in a community-defined test-case and in a previous publication [36]. As shown in Fig. 4, a sample of TACOT of 5 cm is heated on one side at 1644 K for 1 min at atmospheric pressure and cooled down by re-radiation for 1 min. Adiabatic boundary conditions are used at the bottom. The initial conditions are: $p = 1$ atm (101,325 Pa), $T = 300$ K, sample length: 0.05 m. Fig. 5 shows a comparison of the thermal response when using finite-rate chemistry versus equilibrium chemistry. The difference is explained by the fact that the pyrolysis gas enthalpies are significantly different (equilibrium vs. finite-rate). The non-equilibrium enthalpy of the pyrolysis gas mixture produced by the reactions presented in Table 1 is smaller than its equilibrium value. The enthalpy of pyrolysis, that is defined as the difference between solid and gas enthalpies, is therefore higher when considering finite-rate chemistry. This results in increased predicted temperatures in the material.

Fig. 6 shows the evolution of the non-equilibrium pyrolysis gas composition as it is convected through the material towards the surface – in the absence of diffusion here. It is obvious that in this case the finite-rate chemistry model used in the material will have a strong influence on the predicted species in the boundary layer and that the equilibrium assumption would not be correct. It is interesting to note that a large amount of benzene (A1) is injected in the boundary layer according to the finite-rate chemistry model used whereas benzene is not even present when using equilibrium chemistry. The reliability and validity of the chemistry mechanism used for this analysis is questionable. Original experiments are being carried out by the ablation community to develop and validate finite-rate chemistry mechanisms for low density carbon/phenolic ablators [49–51].
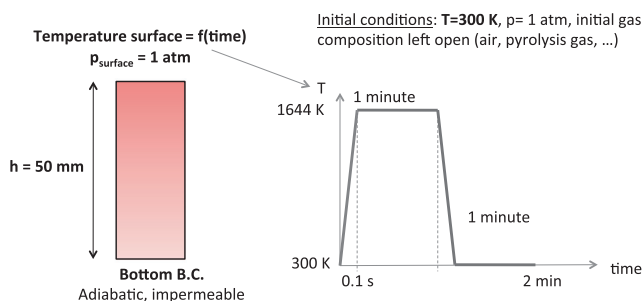

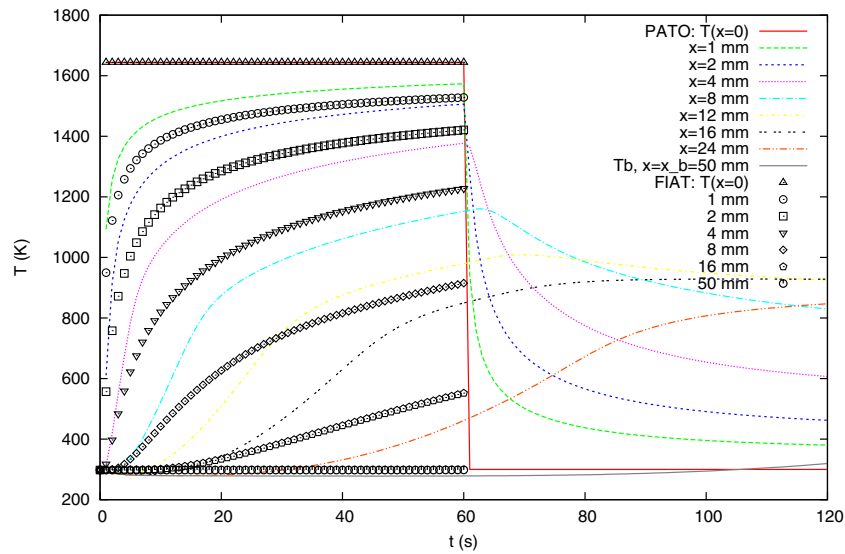Fig. 4. Schematic description of test-case 1.0.

Fig. 5. Test-case 1.0: comparison of thermal response between PATO-type3 and FIAT (type 1).
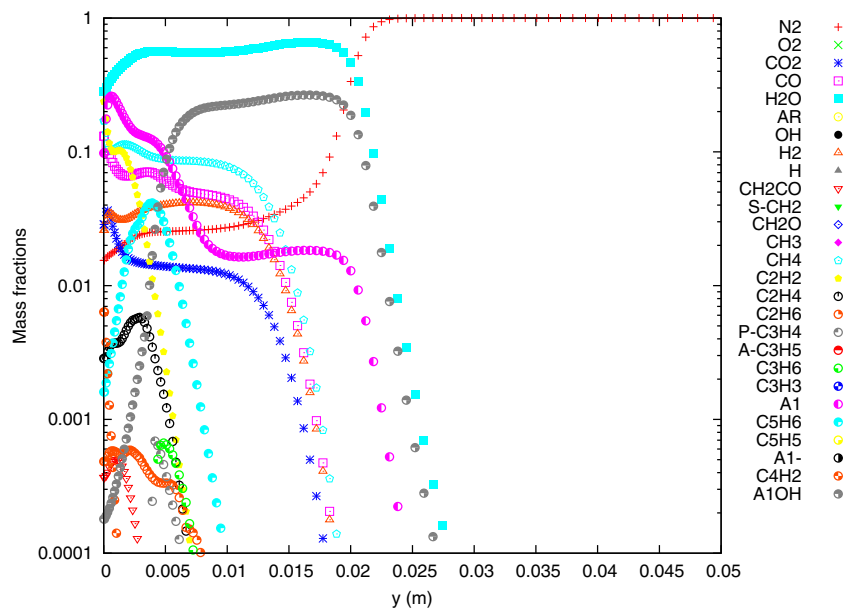

Fig. 6. Test-case 1.0 at 60 s: PATO-type3 – finite-rate chemistry – diffusion neglected [36]. The surface of the sample is in $y = 0$.

3.2. Pyrolysis of lignocellulosic biomass

Pyrolysis is one of the many thermochemical processes available to reduce biomass wastes and/or transform biomass in value-added products [52]. This process has been widely studied in the past [20]. With the climate change concerns, there is currently a renewed interest for this topic, especially for the pyrolysis of lignocellulosic biomass, with wood as an obvious target [23].

There are two types of wood, namely hard wood and soft wood. Softwood consists of long (3–5 mm) cells called tracheids which are about 20–80 µm in diameter. Hard wood can be modeled as an assembly of cells (wood fibers) to which nutrients and water are brought through larger vessels. The micrographs of pyrolyzed Niaouli wood (Melaleuca quinquenervia) from Fig. 7 clearly reveal this hard wood structure. The micrographs have been taken under vacuum with the secondary electron detector of a JOEL JSM IT 300 LVLA scanning electron micrograph at 20 kV. Wood fibers are

elongated quasi-cylindrical cells; their length is of the order of several millimeters, and their diameter is of the order of 10 µm. From a pyrolysis modeling perspective, the content of the cells can be considered to be water. The walls are made of lignocellulose.

As represented in Fig. 8, the core component of lignocellulose is cellulose, a β(1–4)-linked chain of glucose molecules. Hydrogen bonds between different layers of the polysaccharides contribute to the resistance of crystalline cellulose to degradation. Hemicellulose is composed of various 5-and 6-carbon sugars such as arabinose, galactose, glucose, mannose and xylose. Lignin is composed of three major phenolic components, namely p-coumaryl alcohol (H), coniferyl alcohol (G) and sinapyl alcohol (S). Lignin is synthesized by polymerization of these components and their ratio within the polymer varies between different plants, wood tissues and cell wall layers. Cellulose, hemicellulose and lignin form structures called microfibrils, which are organized into macrofibrils that mediate structural stability in the plant cell wall [53].
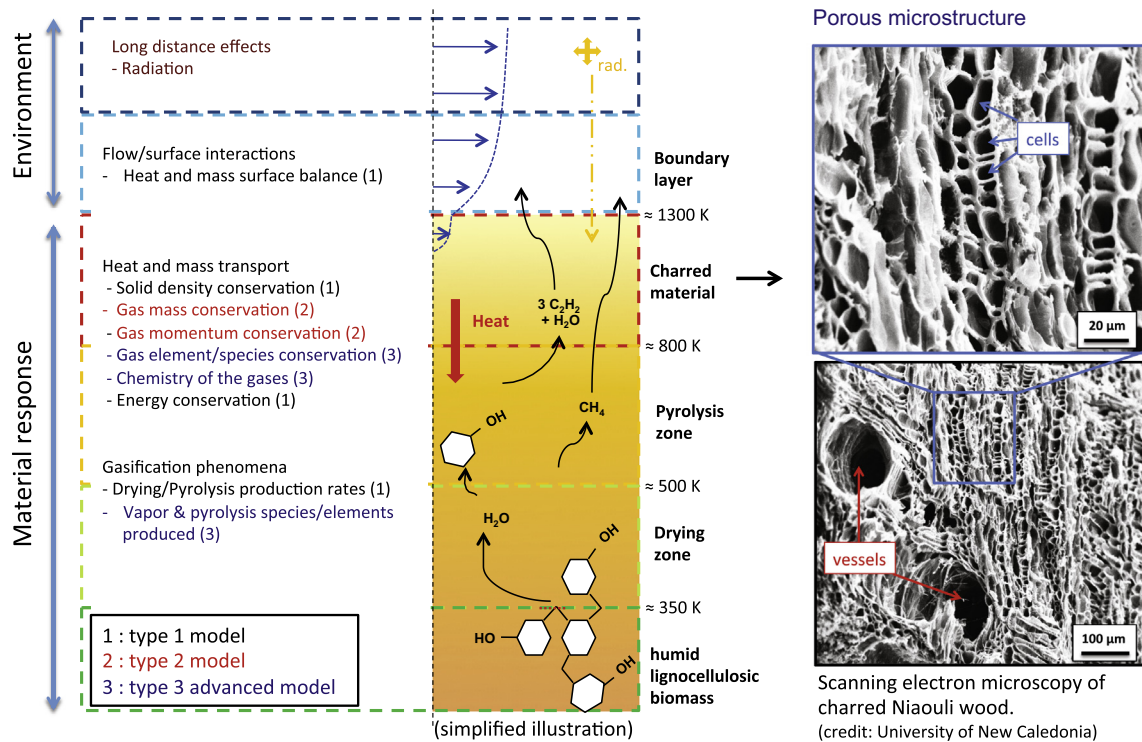
Fig. 7. Phenomenology of wood pyrolysis. On the right: scanning electron micrographs of Niaouli wood from New Caledonia (Melaleuca quinquenervia), pyrolyzed at 500 °C for 15 min, showing empty cells and vessels.
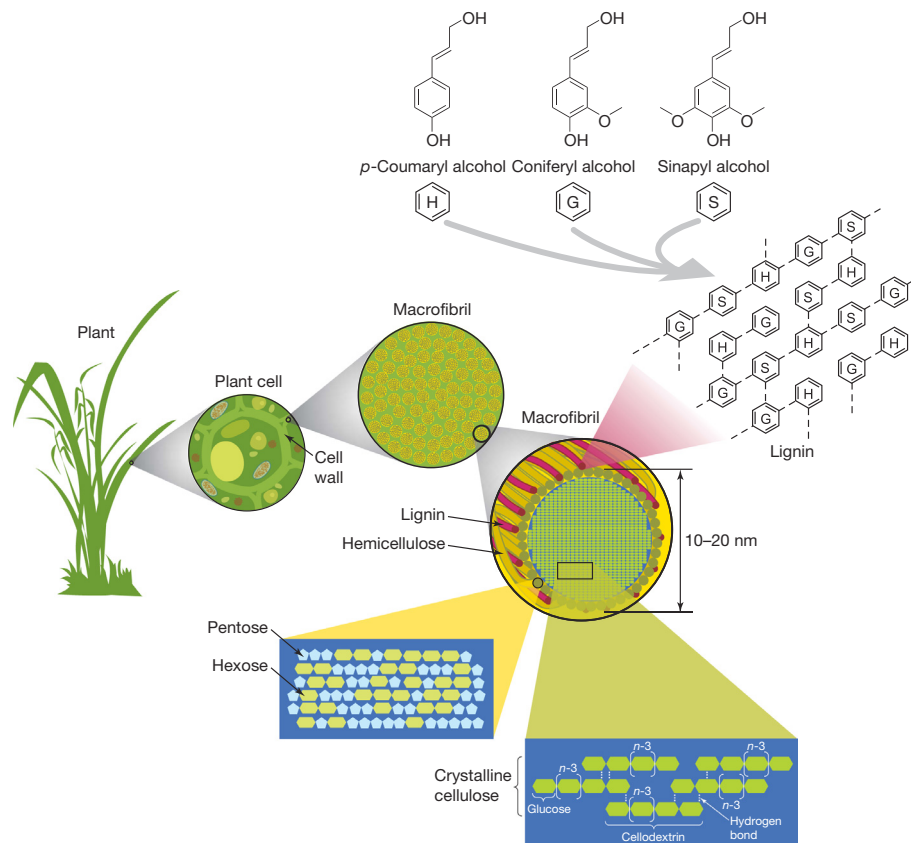

Fig. 8. Representation of the multiscale structure of ligno-cellulosic biomass. Schematic adapted from [53] by [54] with authorization from Nature (open access).
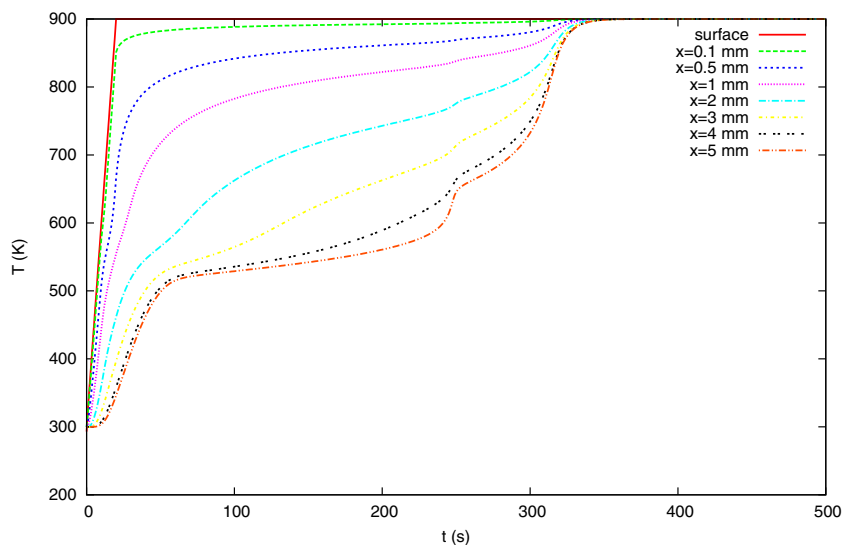
Fig. 9. Simulation of the pyrolysis of a 10 mm Niaouli wood chip at 900 K.

Most pyrolysis studies focus on modeling a chip of wood, non differentiating hard and soft woods and using macroscopic experimental data to model the overall heat transfer and pyrolysis processes. As for ablation, we find different levels of modeling in the literature, not yet categorized but that could fall under the same type 1, type 2, and type 3 nomenclature [20,21], as represented in Fig. 7. Under the effect of heat in the absence of oxygen, wood is first desiccated (10–50% of its initial mass is water). Then it is pyrolyzed. Pyrolysis products are chiefly methane, carbon monoxide and dioxide, hydrogen, condensable gases (like phenol), and tar. The residue is an almost pure carbon char, storing mineral matter (found under the form of ashes after combustion).

The most advanced drying/pyrolysis models consider wood as a N_p solid phase porous medium. The most detailed mechanism available in the literature models the 3 solid phases of lignocellulose, obtained from a compilation of literature data on cellulose, hemicellulose, and lignin decomposition mechanisms [22]. Adsorbed water is conveniently modeled as a fourth phase solid [23]. One added difficulty is to obtain reliable thermochemical data for the wood species studied. Experimentally, effective properties are obtained in virgin and char states. Linear interpolation is used between these two states. Decomposing wood data are estimated by interpolation between virgin and char state measured values [23].

We present below a simulation of Niaouli pyrolysis using the generic model of Section 2. From similar species, we estimated the solid mass fractions to be 37% of cellulose, 20% of hemicellulose, and 43% of lignin. A humidity ratio of 20% has been accounted for under the form of adsorbed water. As a first approximation we used beech wood thermochemical properties [23], because data on Niaouli are not yet available. In this simulation, we used the equilibrium chemistry assumption, and elemental pyrolysis gas mass fractions of C: 0.236, H: 0.413, O: 0.301, N: 0.05. We used the geometry and boundary conditions of the ablation test-case 1.0 presented in the previous subsection, with a surface temperature of 900 K kept at the plateau for 8 min. The results are represented on Fig. 9; several steps are observed corresponding to water vaporization, pyrolysis of hemicellulose, pyrolysis of cellulose, and finally pyrolysis of lignin. We see that according to the simulation it takes about 6 min to fully pyrolyze the wood chip. This is in qualitative agreement with experimental observations [20,22,23].

Depending on the heating rate, temperature, pressure, and ratio of cellulose-hemicellulose-lignin, one may produce different qualities and ratios of char/gas/oil. This is an appealing challenge for the sustainable energy community but it is hard to model due to the lack of quantitative experimental data [55]. Detailed experimental characterizations of the properties of the materials, of the nature of the gases produced by pyrolysis, added to an analysis of the heterogeneous and homogeneous chemistry occurring within the pores, will be needed in order to predict with some degree of accuracy the nature of the gases and bio-oils produced and help optimize industrial processes. To help in this direction, the generic model presented in this article can be used to extract relevant data from elementary experiments as well as contribute to the understanding of overall physical phenomena and couplings.

4. Conclusion

A generic thermal equilibrium model for decomposing and reacting porous materials, containing several solid phases and a single gas phase in the continuum regime (small Knudsen number), has been developed. It provides a general polyvalent framework for detailed engineering analyses, allowing to address various problems with different levels of modeling accuracy. The model has been implemented in PATO, a simulation code released Open Source by the NASA Ames Research Center.[1] The capabilities of the generic model and simulation tool have been presented for two diverse applications: ablative materials and biomass pyrolysis. In the first application, a detailed finite-rate chemistry model was compared to the NASA state-of-the-art equilibrium chemistry model. It was shown that non-equilibrium chemistry can potentially play a significant role in the thermal response of the material and significantly modify the species mixture released in the boundary layer. In the second application, the pyrolysis of a wood chip of Niaouli has been modeled under the equilibrium chemistry assumption. The detailed chemistry capabilities of the model could help understand and optimize the production of hydrocarbon bio-products. For both applications and expectedly for many others, the generic model presented can be used to develop and validate detailed thermochemical models, analyze thermochemical phenomena and couplings, reduce design margin and optimize processes. It is obvious that the generic model would need to be upgraded in some cases, to account for example for local thermal disequilibrium or gas rarefaction effects.

---

[1] https://software.nasa.gov/software/ARC-16680-1, retrieve Jan 1, 2016.

Appendix A. Sublimation *reactivities*

Sublimation is not a chemical reaction but a heterogenous heat-activated species production process, controlled by the partial pressure of the gas species and the local temperature. It is however of great convenience to resolve sublimation coupled with homogeneous and heterogeneous reactions.

Sublimation involves the transition from solid phase to gas phase of an element A as

$$iA_{(s)} \underset{k_i''}{\overset{k_i'}{\rightleftharpoons}} A_i \tag{24}$$

Let us assume the existence of equivalent forward and backward reaction rates, k_i' and k_i'' respectively.

According to the model of Knudsen-Langmuir, the total molar production rate of gaseous species A_i is given by

$$\omega_i = s_i \theta_i \sqrt{\frac{\mathcal{R}T}{2\pi \mathcal{M}_{A_i}}} [X_i^{eq} - X_i] \tag{25}$$

where X_i^{eq} is the equilibrium partial pressure of species A_i, and X_i is its mole fraction in the gas phase.

By identification with Eqs. (10) and (9), we obtain the equivalent forward and backward sublimation *reactivities*

$$k_i' = \frac{\epsilon_g}{\rho_g i} \sqrt{\frac{\mathcal{R}T}{2\pi \mathcal{M}_{A_i}}} X_i^{eq} \tag{26}$$

$$k_i'' = \frac{\sigma_i \theta_i}{i} \sqrt{\frac{\mathcal{R}T}{2\pi \mathcal{M}_{A_i}}} \tag{27}$$

Appendix B. Multicomponent diffusion with strong temperature and pressure gradients

The problem studied involves strong gradients of species concentration, temperature, and pressure. Multicomponent diffusion is potentially an important contributor to mass transport. A very convenient method that uses driving forces to estimate the bulk diffusion fluxes of mass $\mathcal{F}_i^*$ and energy $\mathcal{Q}_i^*$, when conserving either the species or the elements, was recently derived [56]. The idea is to use the rigorous Maxwell model, while simplifying its integration in the conservation equations by precomputing driving forces attributed to the pressure, temperature, and species mole fraction gradients. In the continuum regime (small Knudsen number), a simple correction, inspired from the binary mixtures theory [4], may be used as a first approximation to account for the porosity ϵ_g and the tortuosity η of the porous medium of interest. It reads

$$\mathcal{F}_i = \frac{\epsilon_g}{\eta} \mathcal{F}_i^* \tag{28}$$

$$\mathcal{Q}_i = \frac{\epsilon_g}{\eta} \mathcal{Q}_i^* \tag{29}$$

For a gas in local thermal equilibrium with no electric field, bulk diffusion fluxes are given by [33]

$$\mathcal{F}_i^* = -y_i \rho_g \sum_{j \in N_g^s} D_{ij} \left(\partial_x x_j + \frac{x_j - y_j}{p} \partial_x p + \frac{k_{T_j}}{T} \partial_x T \right) \tag{30}$$

with D_{ij} the multicomponent diffusion coefficient for species i and j, and k_{T_j} the thermal diffusion coefficient of species j. From the above, it is clear that the mass diffusion fluxes for each species may be easily written in terms of gradients of pressure, temperature, and species mole fractions such that

$$\mathcal{F}_i^* = \mathcal{F}_i^p \partial_x p + \mathcal{F}_i^T \partial_x T + \sum_{j \in N_g^s} \mathcal{F}_i^{x_j} \partial_x x_j \tag{31}$$

where the driving forces are given by

$$\mathcal{F}_i^p = -y_i \rho_g \sum_{j \in N_g^s} D_{ij} \frac{x_j - y_j}{p}$$

$$\mathcal{F}_i^T = -y_i \rho_g \sum_{j \in N_g^s} D_{ij} \frac{k_{T_j}}{T} \tag{32}$$

$$\mathcal{F}_i^{x_j} = -y_i \rho_g D_{ij}$$

When the characteristic time of the chemical reactions is much smaller than the characteristic flow time, the mixture can be modeled in chemical equilibrium, and only the element continuity Eqs. (15) need to be satisfied. Each species i in the mixture carries v_i^k atoms of element k. Therefore, the density of each element k in the mixture is determined by summing over the species densities such that

$$z_k = \sum_{i \in N_g^s} y_i v_i^k \frac{\mathcal{M}_k}{\mathcal{M}_i} \tag{33}$$

The bulk diffusion flux of each element is given by

$$\mathcal{F}_k^* = -\sum_{i \in N_g^s} y_i \rho_g v_i^k \frac{\mathcal{M}_k}{\mathcal{M}_i} \sum_{j \in N_g^s} D_{ij} \left(\partial_x x_j + \frac{x_j - y_j}{p} \partial_x p + \frac{k_{T_j}}{T} \partial_x T \right) \tag{34}$$

At equilibrium, the species mole fractions are functions of the mixture temperature, pressure, and element mole fraction w_k

$$x_j = x_j(T, p, w_k), \tag{35}$$

therefore we can use the chain rule to write the species mole fraction gradient as

$$\partial_x x_j = \frac{\partial x_j}{\partial p} \partial_x p + \frac{\partial x_j}{\partial T} \partial_x T + \sum_{l \in N_g^e} \frac{\partial x_j}{\partial w} \partial_x w_l \tag{36}$$

Substituting this expression into the elemental diffusion flux equation, we may write the elemental diffusion fluxes as

$$\mathcal{F}_k^* = \mathcal{F}_k^p \partial_x p + \mathcal{F}_k^T \partial_x T + \sum_{l \in N_g^e} \mathcal{F}_k^{w_l} \partial_x w_l \tag{37}$$

where the driving forces are given by

$$\mathcal{F}_k^p = -\sum_{i \in N_g^s} y_i \rho_g \frac{\mathcal{M}_k}{\mathcal{M}_i} v_i^k \sum_{j \in N_g^s} D_{ij} \left(\frac{\partial x_j}{\partial p} + \frac{x_j - y_j}{p} \right)$$

$$\mathcal{F}_k^T = -\sum_{i \in N_g^s} y_i \rho_g \frac{\mathcal{M}_k}{\mathcal{M}_i} v_i^k \sum_{j \in N_g^s} D_{ij} \left(\frac{\partial x_j}{\partial T} + \frac{k_{T_j}}{T} \right) \tag{38}$$

$$\mathcal{F}_k^{w_l} = -\sum_{i \in N_g^s} y_i \rho_g \frac{\mathcal{M}_k}{\mathcal{M}_i} v_i^k \sum_{j \in N_g^s} D_{ij} \frac{\partial x_j}{\partial w_l}$$

The diffusive energy fluxes are obtained by multiplying the mass fluxes by the mass enthalpy such that, using the same procedure, we obtain

$$\sum_{i \in N_g^s} (\mathcal{Q}_i^*) = \mathcal{F}_h^p \partial_x p + \mathcal{F}_h^T \partial_x T + \sum_{j \in N_g^\xi} \mathcal{F}_h^{\xi_j} \partial_x \xi_j \tag{39}$$

where ξ represents either the species or element model fractions depending on which model is being used and the set N_g^ξ represents either the set of species or elements.

When the species continuity equation are being solved, the factors in the diffusive energy flux equation are given by

$$\mathcal{F}_h^p = -\sum_{i\in N_g^s} y_i \rho_g h_i \sum_{j\in N_g^s} D_{ij} \frac{x_j - y_j}{p}$$

$$\mathcal{F}_h^T = -\sum_{i\in N_g^s} y_i \rho_g h_i \sum_{j\in N_g^s} D_{ij} \frac{k_{T_j}}{T} \qquad (40)$$

$$\mathcal{F}_h^{x_j} = -\sum_{i\in N_g^s} y_i \rho_g h_i D_{ij}$$

When chemical equilibrium is assumed, the energy diffusive flux factors are

$$\mathcal{F}_h^p = -\sum_{i\in N_g^s} y_i \rho_g h_i \sum_{j\in N_g^s} D_{ij} \left(\frac{\partial x_j}{\partial p} + \frac{x_j - y_j}{p} \right)$$

$$\mathcal{F}_h^T = -\sum_{i\in N_g^s} y_i \rho_g h_i \sum_{j\in N_g^s} D_{ij} \left(\frac{\partial x_j}{\partial T} + \frac{k_{T_j}}{T} \right) \qquad (41)$$

$$\mathcal{F}_h^{w_l} = -\sum_{i\in N_g^s} y_i \rho_g h_i \sum_{j\in N_g^s} D_{ij} \frac{\partial x_j}{\partial w_l}$$

The driving forces and the energy factors can be provided by the open source software Mutation++ [31].

Appendix C. Boundary conditions

The generic porous medium model presented allows modeling a large range of problems. Each problem features specific material/environment interactions that are captured by boundary conditions. Boundary conditions are needed for unknown variables that are discretized in space and that cannot be explicitly obtained from other known variables. These variables are found in the continuity equations: species or element mass fractions (conservation of mass, Eq. (14) or (15)), pressure (conservation of momentum, Eq. (18)), and local thermal equilibrium temperature (conservation of energy, Eq. (23)). One specificity of the homogenized model is that the gas velocity is directly given by the pressure gradient (Darcy's law). No velocity boundary condition is required even for inflow boundary conditions.

For partial differential equations, boundary conditions can either be provided as the values (Dirichlet boundary condition) or as the derivatives (Neumann boundary condition) that the solution takes along the boundary of the domain. In this theoretical work, we used Dirichlet boundary conditions for both applications (imposed surface temperature and pressure). Practically, boundary values are not trivial to obtain. When they cannot be experimentally measured, energy and/or mass balances need to be solved along the boundary of the domain. These mass and energy balances are very dependent on the application of interest and on the desired level of accuracy. For the interested reader, examples of detailed mass and energy balance for the heat shield application are provided in Ref. [15].

References

[1] H. Darcy, Les fountains publiques de la ville de Dijon, Librairie des corps impériaux des ponts et chaussées et des mines, Paris, 1856.
[2] E. Sanchez-Palencia, On the asymptotics of the fluid flow past an array of fixed obstacles, Int. J. Eng. Sci. 20 (1982) 1291–1301.
[3] S. Whitaker, Flow in porous media I: a theoretical derivation of Darcy's law, Transp. Porous Media 1 (1986) 3–25.
[4] S. Whitaker, The Method of Volume Averaging, Kluwer Academic Publisher, Dordrecht, The Netherlands, 1999.
[5] D.A. Nield, A. Bejan, Convection in Porous Media, third ed., Springer, New-York, 2006.
[6] M.F. Modest, Radiative Heat Transfer, second ed., McGraw-Hill, New York, 1993.
[7] J. Quintard, Introduction to heat and mass transport in porous media, in: O. Chazot, F. Panerai (Eds.), Porous Media Interaction with High Temperature and High Speed Flows, NATO, Science and Technology Organization, STO-AVT-261, Paris, France, 2015, p. 42.
[8] G.L. Vignoles, Reactive processes in high temperature porous materials, in: O. Chazot, F. Panerai (Eds.), Porous Media Interaction with High Temperature and High Speed Flows, NATO, Science and Technology Organization, STO-AVT-261, Paris, France, 2015, p. 22.
[9] J. Taine, F. Enguehard, Characterization of the radiative properties of homogeneous, anisotropic or non homogeneous porous media, in: O. Chazot, F. Panerai (Eds.), Porous Media Interaction with High Temperature and High Speed Flows, NATO, Science and Technology Organization, STO-AVT-261, Paris, France, 2015, p. 22.
[10] F. Topin, Non-darcian phenomena in porous media, in: O. Chazot, F. Panerai (Eds.), Porous Media Interaction with High Temperature and High Speed Flows, NATO, Science and Technology Organization, STO-AVT-261, Paris, France, 2015, p. 62.
[11] F. Panerai, X-ray microtomography of porous materials, in: O. Chazot, F. Panerai (Eds.), Porous Media Interaction with High Temperature and High Speed Flows, NATO, Science and Technology Organization, STO-AVT-261, Paris, France, 2015, p. 22.
[12] J.C. Ferguson, F. Panerai, J. Lachaud, A. Martin, S.C. Bailey, N.N. Mansour, Modeling the oxidation of low-density carbon fiber material based on micro-tomography, Carbon 96 (2016) 57–65, http://dx.doi.org/10.1016/j.carbon.2015.08.113.
[13] R.M. Kendall, E.P. Bartlett, R.A. Rindal, C.B. Moyer, An analysis of the coupled chemically reacting boundary layer and charring ablator: Part I, NASA CR 1060 (1968) 1–96.
[14] N. Puiroux, M. Prat, M. Quintard, Non-equilibrium theories for macroscale heat transfer: ablative composite layer system, Int. J. Therm. Sci. 43 (6) (2004) 541–554.
[15] J. Lachaud, T. van Eekelen, J.B. Scoggins, T.E. Magin, N.N. Mansour, Detailed chemical equilibrium model for porous ablative materials, Int. J. Heat Mass Transfer 90 (2015) 1034–1045, http://dx.doi.org/10.1016/j.ijheatmasstransfer.2015.05.106.
[16] N. Gascoin, High temperature and pressure reactive flows through porous media, Int. J. Multiph. Flow 37 (1) (2010) 24–35, http://dx.doi.org/10.1016/j.ijmultiphaseflow.2010.09.001.
[17] R.A. Rindal, K.J. Clark, C.B. Moyer, D.T. Flood, Experimental and theoretical analysis of ablative material response in liquid-propellant rocket engine, NASA CR 72301 (1967) 1–230.
[18] V. Borie, J. Brulard, G. Lengellé, An areothermochemical analysis of carbon-carbon nozzle regression in solid-propellant rocket motors, J. Propul. Power 5 (6) (1989) 665–673, http://dx.doi.org/10.2514/3.23204.
[19] G. Vignoles, Y. Aspa, M. Quintard, Modelling of carbon-carbon composite ablation in rocket nozzles, Compos. Sci. Technol. 70 (9) (2010) 1303–1311, http://dx.doi.org/10.1016/j.compscitech.2010.04.002.
[20] C.D. Blasi, Modeling chemical and physical processes of wood and biomass pyrolysis, Prog. Energy Combust. Sci. 34 (2008) 47–90, http://dx.doi.org/10.1016/j.pecs.2006.12.001.
[21] J. Ratte, F. Marias, J. Vaxelaire, P. Bernada, Mathematical modelling of slow pyrolysis of a particle of treated wood waste, J. Hazard. Mater. 170 (1) (2009) 1023–1040.
[22] W.C. Park, A. Atreya, H.R. Baum, Experimental and theoretical investigation of heat and mass transfer processes during wood pyrolysis, Combust. Flame 157 (2010) 481–494.
[23] V. Pozzobon, S. Salvador, J.J. Béziana, M. El-Hafi, Y.L. Maoult, G. Flamant, Radiative pyrolysis of wet wood under intermediate heat flux: experiments and modelling, Fuel Process. Technol. 128 (2014) 319–330.
[24] G.F. Sykes, Thermal cracking of phenolic-nylon pyrolysis products on passing through a heated char, NASA TN D-5804 (1967) 1–19.
[25] G. Fau, N. Gascoin, P. Gillard, M. Bouchez, J. Steelant, Fuel pyrolysis through porous media: coke formation and coupled effect on permeability, J. Anal. Appl. Pyrol. 95 (2012) 180–188, http://dx.doi.org/10.1016/j.jaap.2012.02.005.
[26] L. Romagnosi, N. Gascoin, E. El-Tabach, I. Fedioun, M. Bouchez, J. Steelant, Pyrolysis in porous media: Part 1. Numerical model and parametric study, Energy Convers. Manage. 68 (1) (2013) 63–67, http://dx.doi.org/10.1016/j.enconman.2012.12.023.
[27] G.L. Vignoles, F. Langlais, C. Descamp, A. Mouchon, A. Mouchon, H.L. Poche, N. Reuge, N. Bertrand, CVD and CVI of pyrocarbon from various precursors, Surf. Coat. Technol. 188–189 (2004) 241–249.
[28] G. Vignoles, J. Goyhénèche, P. Sebastian, J.R. Puiggali, J. Lines, J. Lachaud, P. Delhaes, M. Trinquecostes, The film-boiling densification process for C/C composite fabrication: from local scale to optimization, Chem. Eng. Sci. 61 (17) (2006) 5636–5653, http://dx.doi.org/10.1016/j.ces.2006.04.025.
[29] G. Dagan, S.P. Neuman, Subsurface Flow and Transport: A Stochastic Approach, Cambridge University Press, Cambridge, 1997.
[30] J. Lachaud, I. Cozmuta, N.N. Mansour, Multiscale approach to ablation modeling of phenolic impregnated carbon ablators, J. Spacecraft Rockets 47 (6) (2010) 910–921, http://dx.doi.org/10.2514/1.42681.

[31] J.B. Scoggins, T.E. Magin, Development of Mutation++: multicomponent thermodynamic and transport property library for ionized plasmas written in C++, AIAA Pap. 2966 (2014) 1–15, http://dx.doi.org/10.2514/6.2014-2966.

[32] J.B. Scoggins, T.E. Magin, Gibbs function continuation for linearly constrained multiphase equilibria, Combust. Flame 162 (2015) 4514–4522, http://dx.doi.org/10.1016/j.combustflame.2015.08.027.

[33] V. Giovangigli, Multicomponent Flow Modeling, Birkhäuser, Boston, 1999.

[34] H.J. Ene, E. Sanchez-Palencia, On thermal equation for flow in porous media, Int. J. Eng. Sci. 20 (5) (1982) 623–630.

[35] T. van Eekelen, J. Lachaud, Numerical validation of an effective radiation heat transfer model for fiber preforms, J. Spacecraft Rockets 48 (3) (2011) 534–537, http://dx.doi.org/10.2514/1.51865.

[36] J. Lachaud, N.N. Mansour, Porous material analysis toolbox based on openfoam and applications, J. Thermophys. Heat Transfer 28 (2) (2014) 191–202, http://dx.doi.org/10.2514/1.T4262.

[37] H. Jasak, Error analysis and estimation for the finite volume method with applications to fluid flows (Ph.D. thesis), Imperial College London (University of London), 1996.

[38] H.G. Weller, G. Tabor, H. Jasak, C. Fureby, A tensorial approach to computational continuum mechanics using object-oriented techniques, Comput. Phys. 12 (6) (1998) 620–631.

[39] J.D. Anderson, Hypersonic and High Temperature Gas Dynamics, Mac Graw-Hill, New-York, 1989.

[40] G. Duffa, Ablative thermal protection systems modeling, AIAA Educ. Ser. (2013), http://dx.doi.org/10.2514/4.101717.

[41] M. Stackpoole, S. Sepka, I. Cozmuta, D. Kontinos, Post-flight evaluation of stardust sample return capsule forebody heatshield material, AIAA Pap. 1202 (2008) 1–7.

[42] M.J. Wright, R. Beck, K. Edquist, D. Driver, S. Sepka, E. Slimko, W. Willcockson, Sizing and margins assessment of the mars science laboratory aeroshell thermal protection system, J. Spacecraft Rockets 51 (4) (2014) 1125–1138, http://dx.doi.org/10.2514/1.A32579.

[43] J. Lachaud, T. Magin, I. Cozmuta, N.N. Mansour, A short review of ablative material response models and simulation tools, in: L. Ouwehand (Ed.), Proceedings of the 7th European Symposium on Aerothermodynamics, SP-692, European Space Agency, Noordwijk, The Netherlands, 2011, pp. 1–12, ISBN: 978-92-9221-256-8.

[44] C.B. Moyer, R.A. Rindal, An analysis of the coupled chemically reacting boundary layer and charring ablator: Part II, NASA CR 1061 (1968) 1–168.

[45] Y.K. Chen, F.S. Milos, Ablation and thermal response program for spacecraft heatshield analysis, J. Spacecraft Rockets 36 (3) (1999) 475–483.

[46] M.A. Covington, J.M. Heinemann, Y.-K. Chen, I. Terrazas-Salinas, J.A. Balboni, J. Olejniczak, E.R. Martinez, Performance of a low density ablative heat shield material, J. Spacecrafts Rockets 45 (4) (2008) 856–864.

[47] F. Milos, Y.-K. Chen, Ablation and thermal response property model validation for phenolic impregnated carbon ablator, J. Spacecrafts Rockets 47 (5) (2010) 786–805.

[48] H.K. Tran, C.E. Johnson, D.J. Rasky, F.C.L. Hui, M.-T. Hsu, T. Chen, Y.K. Chen, D. Paragas, L. Kobayashi, Phenolic impregnated carbon ablators (PICA) as thermal protection systems for discovery missions, NASA Tech. Memorandum 110440 (1997) 1–70.

[49] F. Panerai, A. Martin, N.N. Mansour, S.A. Sepka, J. Lachaud, Flow-tube oxidation experiments on the carbon preform of pica, J. Thermophys. Heat Transfer 40 (2) (2014) 181–190, http://dx.doi.org/10.2514/1.T4265.

[50] H.-W. Wong, J. Peck, R. Bonomi, J. Assif, G. Reinisch, J. Lachaud, N.N. Mansour, Quantitative determination of species production from the pyrolysis of a phenol-formaldehyde resin, Polym. Degrad. Stab. 112 (2015) 122–131, http://dx.doi.org/10.1016/j.polymdegradstabl.2014.12.020.

[51] B.K. Bessire, S.A. Lahankar, T.K. Minton, Pyrolysis of phenolic impregnated carbon ablator (pica), Appl. Mater. Interfaces 3 (7) (2015) 1383–1395, http://dx.doi.org/10.1021/am507816f.

[52] Intergovernmental Panel on Climate Change, Renewable Energy Sources and Climate Change Mitigation, Cambridge University Press, 2011.

[53] E.M. Rubin, Genomics of cellulosic biofuels, Nature 454 (7206) (2008) 841–845.

[54] J.M. Moran-Mirabal, Cellulose – Fundamental Aspects, Intechopen, Ch. I – Advanced-Microscopy Techniques for the Characterization of Cellulose Structure and Cellulose-Cellulase Interactions, 2013, pp. 1–34.

[55] C. Couhert, J.-M. Commandre, S. Salvador, Is possible to predict gas yields of any biomass after rapid pyrolysis at high temperature from its composition in cellulose, hemicellulose and lignin?, Fuel 88 (2009) 408–417

[56] J.B. Scoggins, T.E. Magin, Mutation++ User Manual, 1st ed., von Karman Institute for Fluid Dynamics, Rhode Saint Genese, Belgium, 2015.